J Mater Sci (2009) 44:903–918
DOI 10.1007/s10853-008-3183-z

Effect of polar modification on morphology and properties of styrene-(ethylene-co-butylene)-styrene triblock copolymer and its montmorillonite clay-based nanocomposites

Anirban Ganguly · Anil K. Bhowmick

Received: 10 July 2008 / Accepted: 11 December 2008 / Published online: 31 December 2008

Abstract This article deals with the functionalization of a triblock copolymer, poly-(styrene-ethylene-co-butylene)-styrene (SEBS), at the mid-block by means of chemical grafting by two polar moieties—acrylic acid and maleic anhydride and subsequent novel synthesis of nanocomposites based on hydrophilic montmorillonite clay (MT) at very low loadings. The mid-block was grafted with 3 and 6 wt% acrylic acid through solution grafting and 2 and 4 wt% maleic anhydride through melt grafting reactions which were confirmed by spectroscopic techniques. The nanocomposites derived from the grafted SEBS and hydrophilic MT clay conferred dramatically better mechanical, dynamic mechanical, and thermal properties as compared to those of the original SEBS and its clay-based nanocomposites. Different phase separated morphologies could be observed from transmission electron microscopy (TEM) and atomic force microscopy (AFM) studies for grafted SEBS. X-ray diffraction (XRD), AFM, and TEM studies revealed better interaction and dispersion of MT clays with the grafted SEBS matrix, resulting in better transparency of these nanocomposite films. Superlative enhancement of thermal degradation properties was achieved with maleated and acrylated SEBS–MT nanocomposites. Thermodynamic calculations and interfacial tension measurements indicated possible ways of favorable intercalation-exfoliation mechanism of maleated and acrylated SEBS–MT nanocomposites.

A. Ganguly · A. K. Bhowmick (✉)
Rubber Technology Centre, Indian Institute of Technology, Kharagpur 721302, India
e-mail: anilkb@rtc.iitkgp.ernet.in

Introduction

The nano-science and technology offers unique opportunities to create revolutionary material combinations by a unique synergism between constituting materials. This occurs when the length-scale of the morphology with its fundamental science is associated with a property corresponding to nanoscale [1]. Nanocomposites, therefore, generate a great deal of interest from materials' scientists because of their potentially novel properties.

Polymer nanocomposites are a class of materials in which the dimensions of the reinforcing phase are in the order of nanometers in the polymer matrix [1–3]. Due to the dimensional characteristics, nanocomposites possess superior properties to conventional microcomposites, as they maximize the interfacial adhesion. These properties make them extremely interesting in the field of design and creation of new construction materials [1–5]. The smectite clays as layered silicates are considered to be good candidates for the preparation of organic–inorganic nanocomposites because they can be broken down into nanoscale building blocks resulting in optically transparent hybrids.

The mechanical and thermal properties of polymers are generally improved by the addition of inorganic additives. Since the organic polymer matrix is relatively incompatible with the inorganic phase, improvements in the interfacial adhesion between the polymer matrix and the reinforcing material become a challenge in this area of high-performance organic–inorganic hybrid materials [4, 5]. A better interfacial bonding can impart better properties to a polymer composite where improved attraction between nanofillers and the polymer matrix gives forth better physico-mechanical, thermal, morphological, and optical properties due to a better particulate dispersion in the entire

nanocomposite. The most common type of clay is montmorillonite (MT), a layered aluminosilicate in the smectite family of clays. Unlike clay minerals such as talc, whiting etc. that have been used as fillers for years, MT clays can be delaminated and dispersed into individual layers of minimum 1 nm in thickness. The result is a radical increase in the surface area-to-volume ratio with a maximized surface area as high as 750 m^2/g. When unseparated MT particles (tactoids) are partially separated by polymer chains, they are referred to as being intercalated, while thoroughly separated, individual platelets are said to be exfoliated [1–6]. The incorporation of a very low amount (typically 2–5 wt%) of high surface-area nanoclays into host polymer systems improves the performance of the specific polymer matrix.

These polymer-layered silicate nanocomposites have generated significant interest in academia and industry [1–7] as a result of their enhancement of a wide range of properties containing only a few volume percent of nanofiller. The journey was started in 1990s by the Toyota group in Japan [8]. Having touched upon almost all known polymers, attention has been paid to rubber-based nanocomposites very recently [9]. Such rubber–clay nanocomposites prepared by earlier workers from our laboratory have demonstrated interesting results, which are a function of the rubber, the solvent used for casting, the nature of the clay, and other factors [10–12]. Less attention has been paid so far to the development of nanocomposites based on thermoplastic elastomers or block copolymers. Krishnamoorti and co-workers studied block copolymer-based nanocomposites [13–15]. Recently, various types of block copolymers have attracted much attention as nanoscale materials on their own. Due to the self-assembling characteristics of the block copolymers [16, 17], many interesting phenomena are expected.

The microstructure of a clay–polymer nanocomposite depends on the type of polymer matrix and nano-clay used and the interactions between these two. These interactions in turn depend on the hydrophobicity of the constituents.

The chosen polymer, styrene-ethylene-butylene-styrene (SEBS), being a triblock copolymer, is extensively used as a very good thermoplastic elastomer which is generally obtained through the complete hydrogenation of the middle block of the styrene-butadiene-styrene (SBS) structure [17, 18]. It exhibits rubber-like properties and a melt processability comparable to conventional thermoplastics. This mainly arises from its microphase-separated morphology having hard polystyrene (PS) microdomains, which act as physical crosslinks of high mechanical strength between the elastomeric sequences, while the soft poly(ethylene butylene) (PEB) mid-blocks impart elasticity to the whole system, similar to conventional vulcanized rubbers.

Due to the nonpolar nature of SEBS, workers have found it very difficult to disperse and exfoliate montmorillonite clays (MT) caused by the incompatibility with hydrophilic clay. The versatility of SEBS block copolymers can be significantly improved by grafting functional groups, such as maleic anhydride (MAH), acrylic acid (AA), etc., to the mid-block [17]. Hence, polar modification of SEBS has drawn attention in recent times [19–27]. However, till now, most researchers have concentrated on the modification of SEBS with MAH in organic solution, melt or graft copolymerization of SEBS with methacrylic acid in organic solution or sol–gel process of intercalating clay in SEBS [27]. Only a few studies are available on the clay-based SEBS nanocomposites [27, 28]. The present authors have also published papers in the area of SEBS–MT clay-based nanocomposites [29, 30]. Scheme 1 illustrates the possible two ways of synthesizing SEBS–clay nanocomposites—one by organically modifying the MT clay surface, which is a common trend in the world of polymer–clay nanocomposites in nonpolar polymer matrices, and another by modifying the polymer (SEBS) matrix itself by a grafting reaction so that unmodified MT clay can be used as such. The second approach is new in the context that organic modification of MT clay surface is not required to synthesize grafted SEBS–clay nanocomposite. In this present investigation, we have presented this second approach, which is an entirely new one for intercalating-exfoliating clay platelets of hydrophilic sodium montmorillonite nanoclay (MT) in SEBS matrix. Hydrophilicity was generated by virtue of grafting polar AA and MA moieties onto the polymer and then the MT clay was impregnated in the corresponding matrices.

This is a new approach as all the earlier studies on SEBS–clay nanocomposites have concentrated on intercalating the clay after organically modifying it by long chain amines. Here, unmodified clay has been successfully intercalated and exfoliated by grafted SEBS systems (Scheme 1). The work reported here is concerned with the grafting of SEBS by AA in solution and by MAH in molten state. Subsequent to these graft modifications, preparation

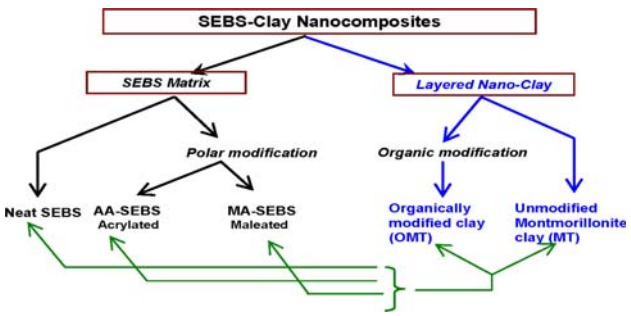

Scheme 1 Interaction scheme of nanocomposite prepared between SEBS and nanoclays

and characteristics of the sodium–MT clay based nanocomposites were prepared in each case, proving that low-cost MT clay can be used in place of organically modified nanoclays.

Experimental

Starting materials

The styrene-ethylene-butylene-styrene triblock copolymer (SEBS) (Kraton G 1652) with a molecular weight $M_w = 57{,}000$ and a styrene/butadiene ratio (w/w) = 30/70 was supplied by Shell Chemical Co, USA. Acrylic acid [CH_2=CH (C=O) OH] (AA, density 1.05 g/cm^3) was procured from Aldrich, USA, and was used after removing the inhibitors by vacuum distillation at its boiling point and reduced pressure. A sample of AA, which was examined under GPC, showed only one peak confirming the purity of the monomer. MAH, benzoyl peroxide (BPO), and dicumyl peroxide (DCP) were supplied by Loba Chemie and Merck India Ltd., Mumbai, India. Toluene (analytical grade) was obtained from Nice Chemicals Pvt. Ltd., Cochin, India. Unmodified sodium montmorillonite clay (MT, having a cation exchange capacity = 92.6 meq/100 g with 2:1 tetrahedral:octahedral layer structure) and long chain quaternary ammonium ion modified nano-clay (OMT) were generously supplied by Southern Clay Products, Gonzales, TX, USA.

Grafting of acrylic acid (AA) onto SEBS

The grafting reaction of AA onto SEBS was performed using BPO as initiator in a solution of SEBS (5%, w/v) in toluene. In total, 5.0 g of SEBS in 100 mL toluene was taken in a three-necked round-bottom flask and was stirred for 1 h. Dry nitrogen (N_2) was passed through the polymer solution in order to drive out the dissolved oxygen present in the solvent and also in the reaction flask. Once the mixture was homogenized, the required amount of AA was added drop-wise to the reaction mixture. After adding AA and homogenizing the mixture, the required amount of BPO was added as initiator. The entire reaction was carried out in N_2 atmosphere. At first, for grafting of AA, the dosage of BPO was optimized with fixed AA concentration and temperature at a specified value of 0.25 wt% with respect to polymer. Thereafter, optimization of the grafting reaction was done at 70 °C and 8 h reaction with varying AA concentration. Finally, the samples were collected and dried under vacuum for 48 h at 40 °C for complete removal of the solvent.

SEBS melt-grafted by MAH

SEBS was melt-grafted by MAH using DCP in a Brabender Plasticorder PL330. The optimal reaction conditions for MAH grafting on SEBS corresponded to a reaction time of 5 min, a reaction temperature of 180 °C, and 6% of MAH, which was effectively grafted up to 4 wt% onto the SEBS backbone using 0.5% DCP.

Measurement of percentage grafting

The grafted SEBS samples were taken in a filter paper and placed in the Sohxlet apparatus for extraction. Each extraction was carried out for 24 h, using water as the extracting medium for complete removal of unreacted AA (or any homopolymer of AA, if at all formed during the reaction) and MAH. After the extraction, the samples wrapped in filter paper were dried under vacuum for 72 h at 70 °C till they showed no weight variation any more. The extent of grafting was calculated from the weight gain by the samples using the following equation:

$$\%\text{Grafting} = \left[\frac{W_g - W_0}{W_0}\right] \times 100 \quad (1)$$

where W_0 is the weight of neat SEBS and W_g the weight of the grafted SEBS.

Film preparation

Films were prepared by casting a SEBS solution (10 g/L in toluene) in a leveled and covered glass petty-dish. The solvent was evaporated for 2 days at room temperature, and the samples were subsequently dried at 80 °C for 2 h in order to remove any solvent trace. The film thickness obtained was typically in the range of 300–500 μm.

Preparation of AA-, MA-SEBS–clay hybrid nanocomposites

AA- and MA-SEBS/clay nanocomposites were prepared using a solvent casting method. Initially, modified SEBS and MT at 2, 4, and 8 wt% and OMT at 4 wt% in appropriate cases were dissolved and dispersed in toluene separately and stirred for 2 h using a magnetic stirrer. The polymer solution and clay particle suspension were then mixed together and stirred for 24 h in order to complete the mixing. Next, the samples were dried in a hood by evaporating the solvent, and the residual solvent and moisture were sequentially removed in a vacuum oven. Grafted SEBS–clay nanocomposites synthesized are charted in Table 1.

Table 1 Grafted SEBS–clay nanocomposites prepared

Polymer matrix	Nanoclay loading	Sample designation
AA3-SEBS	MT-4 wt%	AA3-SEBS-MT4
AA6-SEBS	MT-2 wt%	AA6-SEBS-MT2
	MT-4 wt%	AA6-SEBS-MT4
	MT-8 wt%	AA6-SEBS-MT8
	OMT-4 wt%	AA6-SEBS-OMT4
MA2-SEBS	MT-4 wt%	MA2-SEBS-MT4
	OMT-4 wt%	MA2-SEBS-OMT4
MA4-SEBS	MT-2 wt%	MA4-SEBS-MT2
	MT-4 wt%	MA4-SEBS-MT4
	MT-8 wt%	MA4-SEBS-MT8
	OMT-4 wt%	MA4-SEBS-OMT4

Characterization procedures

Fourier transform infrared (FT-IR) spectroscopic studies

FT-IR studies were carried out in the dispersive mode on Sohxlet extracted thin-film samples using a Perkin Elmer FTIR-spectrophotometer (model Spectrum RX I), within a range of 400–4400 cm^{-1} using a resolution of 4 cm^{-1}. An average of 32 scans have been reported for each sample.

NMR studies

The ^1H NMR spectra of all copolymers containing TMS as an internal standard reference were recorded in deuterated chloroform using a Bruker 400 MHz NMR spectrophotometer at room temperature. All scans were taken after dissolution of the samples in $CDCl_3$.

Measurement of interfacial tension

The *Sessile drop method* was adopted for contact angle measurement [31] using water and formamide as the probe liquids (water: $\gamma_l = 72.8; \gamma_l^d = 21.8; \gamma_l^p = 51.0$. Formamide: $\gamma_l = 58.2;\ \gamma_l^d = 39.5;\ \gamma_l^p = 18.7$ mJ/m^2) [31, 32] in a Kernco (Model G-II) Contact Angle Meter. The polymer plate used in the experiment was of dimension 10 × 10 × 0.5 mm. Each value reported has a maximum error in θ of ±0.2°, and the mean of at least 5 readings was taken.

Interfacial tension was measured for the nanocomposite samples assuming that the polymer spreads clay in the polymer–clay systems, and was calculated using the Fowkes equation [31] and Eq. 2.

$$\gamma_{sc} = \gamma_s + \gamma_c - 2\sqrt{\gamma_s^d \gamma_c^d} - 2\sqrt{\gamma_s^p \gamma_c^p} \quad (2)$$

Wide angle X-ray diffraction studies (WAXD)

Wide angle X-ray diffraction analysis of nanocomposites was carried out in a Pan Analytical XPert Pro 3040/60 X-ray diffractometer (the Netherlands), operated at 30 kV and 40 mA at room temperature, equipped with Cu-K_α radiation.

The scanning rate was 1°/min with the range of Goniometer angle (2θ) 2°–10°. Subsequently, the d-spacing of the clay layers was calculated using the Bragg's equation,

$$n\lambda = 2d \sin\theta \quad (3)$$

where λ is the wavelength of the X-ray with Cu-K_α target = 0.154 nm, d the interplanar distance of the clay platelets, θ is the angle of the incident radiation.

Transmission electron microscopy (TEM)

The samples for the transmission electron microscopy analysis were prepared by ultracryo-microtomy using a Leica Ultracut UCT (Vienna, Austria). Freshly sharpened glass knives with a cutting edge of 45° were used to get the cryosections of 50–70 nm thickness at a sub-ambient temperature of −80 °C using a JEOL 2010 TEM (Japan), operating at an accelerating voltage of 200 kV.

Phase imaging by atomic force microscopy (AFM)

The effects of maleation and AA grafting and inorganic silicate clay phase inclusion in the synthesized nanocomposites on the morphology of the SEBS triblock copolymer were investigated using atomic force microscopy (AFM) in air under ambient conditions (25 °C, 60% RH) using a MultiMode AFM from Digital Instruments (Santa Barbara, CA, USA). Phase detected images were recorded in the Tapping Mode AFM attached with a Nanoscope IIIa feedback controller. The scan angle was slightly rotated and scan speed was also slowly varied without disturbing the image quality to ensure the proper morphology detected by the AFM tip devoid of any tip-artifacts. Phase images were captured in tapping mode using etched silicon probe tips (RTESP), with a spring constant in the range of 40 N/m. For each sample, minimum three images were analyzed.

Dynamic mechanical thermal analysis (DMTA)

The dynamic mechanical spectra of the samples were obtained by using a DMTA of Rheometric Scientific DMTA IV (NJ, USA). The sample specimens (dimension 25 × 10 × 0.4 mm) were analyzed in a tension-compression mode at a constant frequency of 1 Hz, a strain of 0.01%

and a temperature range from −80 to 120 °C at a heating rate of 2 °C/min. The storage modulus (E') and loss tangent (tan δ) were measured as a function of temperature for all samples under identical conditions. The temperature corresponding to the peak in a tan δ versus temperature plot was taken as the glass–rubber transition temperature (T_g).

Studies of mechanical properties

Stress–strain experiments were carried out as per the ASTM D 412 method in a Universal Testing Machine Z010 (Zwick GmbH, Ulm, Germany) at a crosshead speed of 500 mm/min at room temperature (25 ± 2 °C). The average of three tests is reported here with an error of maximum ±5% in each case.

Thermogravimetric analysis (TGA)

The thermogravimetric analysis of SEBS, grafted SEBS, and their nanocomposites was performed with a TGA Q50 of TA Instruments-Waters LLC (USA), operated at a heating rate of 20 °C/min. The samples (∼5 mg) were placed in a platinum pan and the experiments were conducted in N_2 atmosphere at a flow rate of 60 mL/min in the temperature range of 25–700 °C.

Results and discussion

Effect of grafting of AA and MA onto SEBS

Acrylic acid has been grafted onto the SEBS backbone with the optimized 0.25 wt% dosage of BPO at 70 °C for 8 h at varying AA concentrations. Scheme 2a portrays the synthetic route to graft AA into SEBS. Percent weight variation, infrared spectroscopy, NMR, static contact angle measurement, and chemical analyses were used to characterize AA grafted SEBS. Details of the composition of the samples are provided in Table 2. The results of IR and NMR spectra (Figs. 1, 2, and 3) show that AA is successfully grafted onto the SEBS backbone. FTIR spectra as shown in Fig. 1 illustrate the effect of the AA concentration on progressive grafting of the AA moiety onto SEBS. The characteristic peaks for SEBS at 1600 cm^{-1} for aromatic systems remain with the same intensity for all samples. The peak at 699 cm^{-1} for the styrenic moiety of SEBS has shown to remain unchanged with its position and intensity even after the grafting reaction with AA. It gives a proof that the grafting reaction has not taken place in the hard styrenic segment of this block copolymer, SEBS. The peaks at 1712 cm^{-1} for the carbonyl group (C=O) and at 1247 cm^{-1} characteristic for the C–O stretching vibration of a carbonyl group are caused by the grafted AA in the samples. The intensity of these two peaks has proportionately increased for 3 and 6 wt% grafting of AA in SEBS, as shown in the normalized (with respect to 1600 cm^{-1}) FTIR spectra in Fig. 1. The NMR peak at 1.57 confirms grafting of the AA moiety (Fig. 3, discussed later) onto SEBS. Peak area calculation confirms the afore-mentioned result.

Table 2 Grafting of SEBS

Grafting	%Grafting on SEBS (wt%)	Sample designation
Acrylic acid	3	AA3-SEBS
	6	AA6-SEBS
Maleic anhydride	2	MA2-SEBS
	4	MA4-SEBS

Earlier studies by Ghosh et al. [33] had shown grafting of LDPE with AA. Sen et al. [34] and Lim et al. [28] demonstrated grafting copolymerization of polyolefins. In the present study, AA has been solution grafted onto the PEB mid-block of SEBS (having a 2°H, which can be displaced by the acrylic acid).

Scheme 2b shows the optimal reaction condition of MAH melt grafting on SEBS corresponding to a reaction

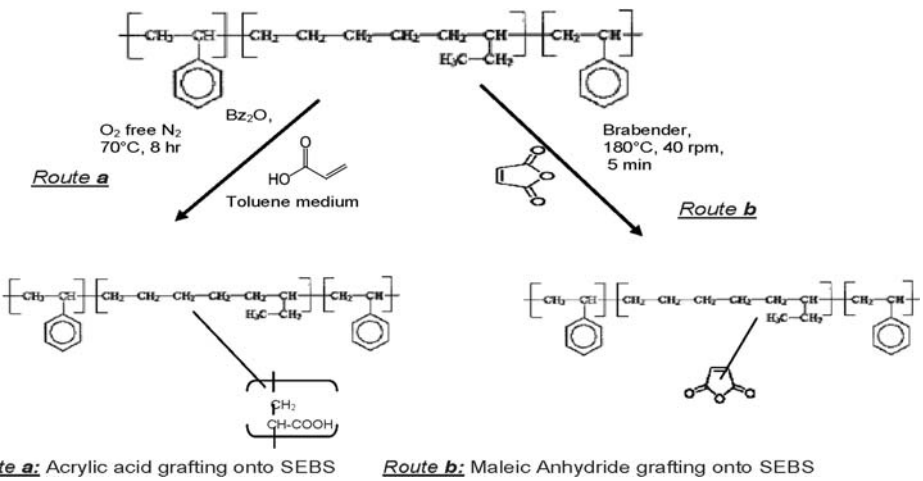

Scheme 2 Synthetic routes to **a** acrylic acid and **b** maleic anhydride grafting onto SEBS

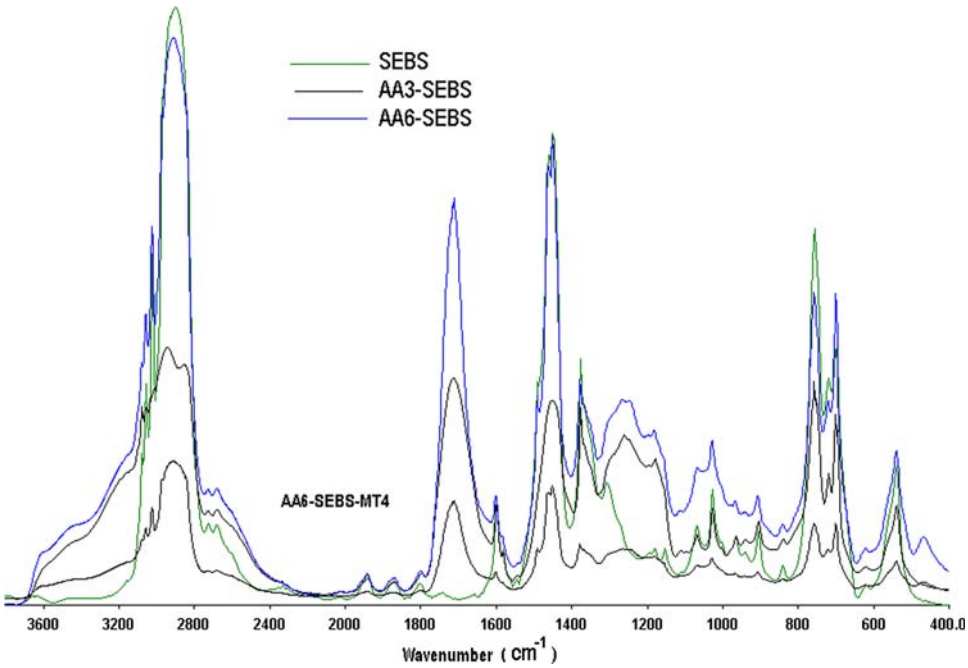

Fig. 1 FTIR traces of neat SEBS and AA grafted SEBS along with AA6-SEBS-MT4 nanocomposite

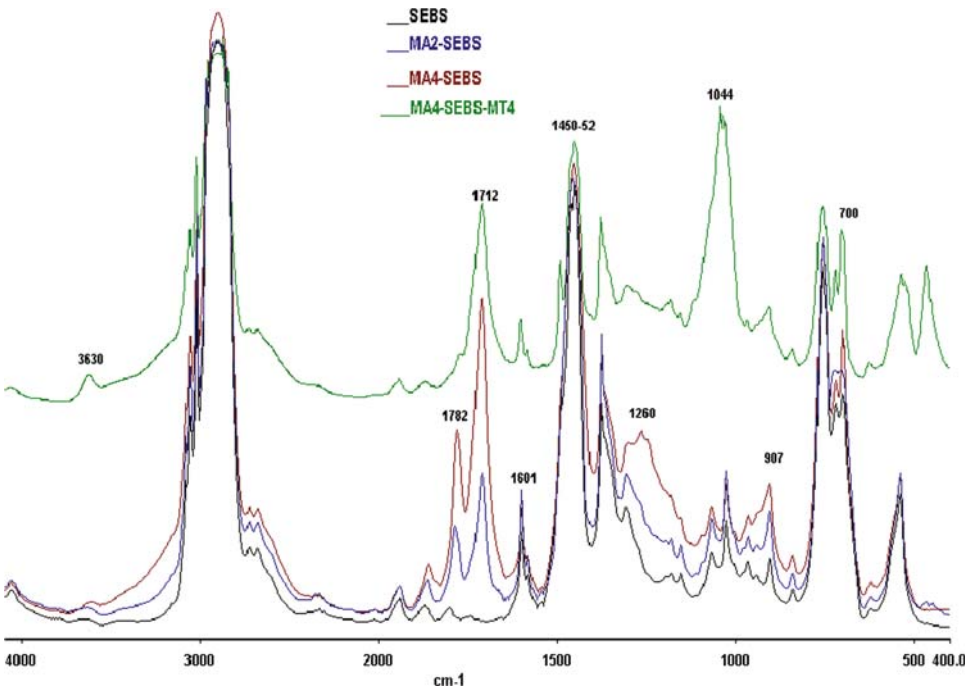

Fig. 2 FTIR traces of neat SEBS and MA melt-grafted SEBS along with MA4-SEBS-MT4 nanocomposite

time of 5 min, a reaction temperature of 180 °C with 0.5 wt% of DCP. A total of 6 and 10% of MAH initially added were effectively grafted at 2 and 4 wt% level, respectively, to the SEBS backbone. MAH has reacted with the secondary carbon of the EB-block at the temperature of melt blending (180 °C). The percentage of grafting of MAH onto the SEBS backbone under optimized reaction conditions has been determined by FT-IR and elemental analysis and is presented in Table 2. From the results of FT-IR and NMR, it is proven that MAH has indeed been grafted on an aliphatic part (i.e. PEB segment) of the SEBS molecular chains and the form of MAH grafting is unimolar. The peaks at 1712 cm^{-1} for carbonyl and 1782 cm^{-1} for succinoyl groups resulting from opening of the MAH ring at high temperature and grafting can be viewed from normalized (wrt. 1600 cm^{-1}) FTIR spectra for MAH grafted to SEBS in Fig. 2. The peak at 1250 cm^{-1} for the C–O stretching vibration (Table 3) is increasing on a

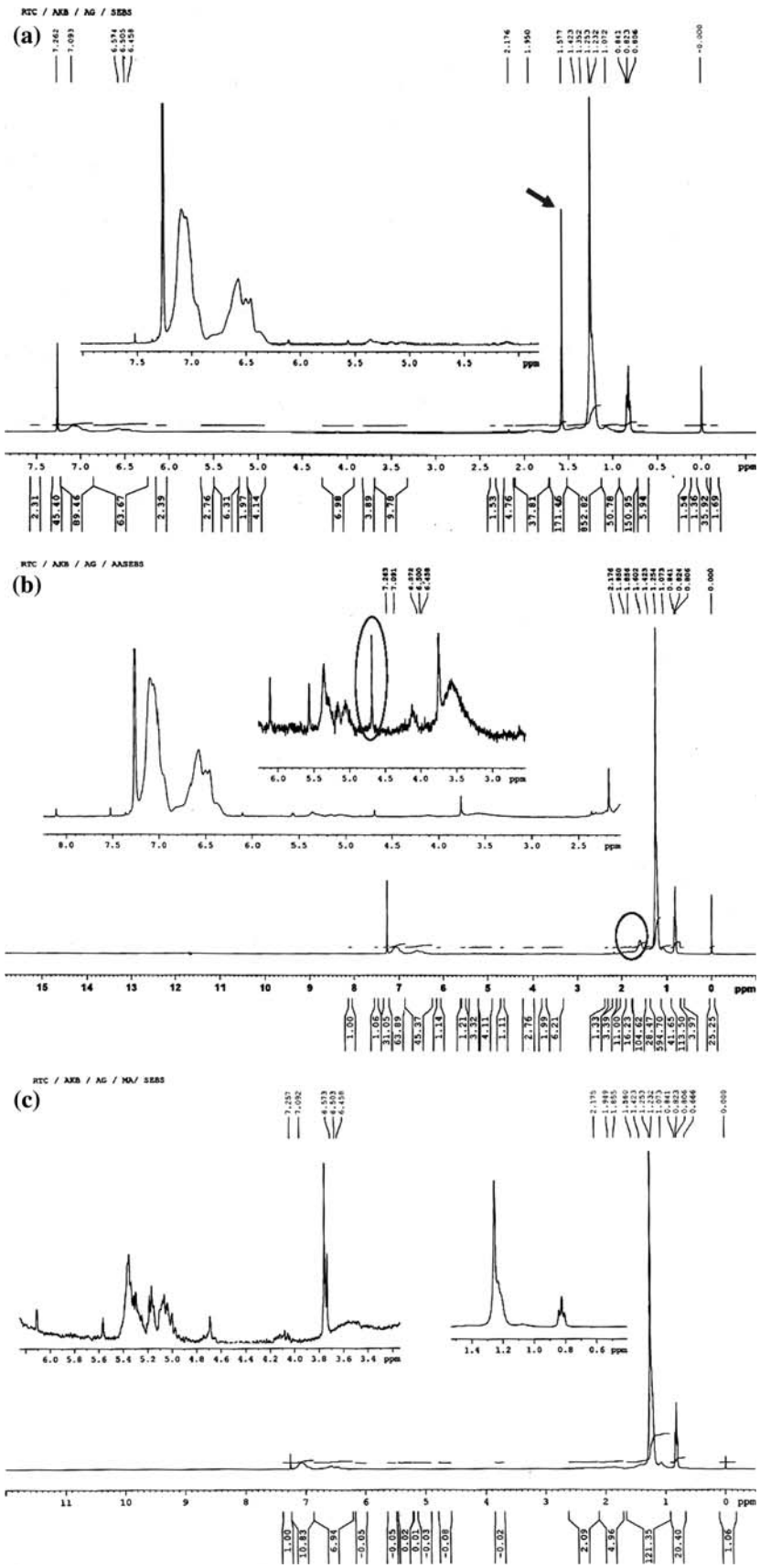

Fig. 3 ^{1}H NMR traces of **a** pristine SEBS and **b** AA-g-SEBS, **c** MA-g-SEBS showing grafting has occurred at aliphatic moiety

Table 3 FT-IR peaks and their description

Peak position (cm^{-1})	Peak description
Broadband near 3440	–OH stretching and intermolecular hydrogen bonded –OH
2920	$–CH_2$ stretching
2850	–NCH and CH_3 stretching
1712 or 1713	C=O peak for maleic anhydride or acrylic acid
1600	Characteristics peak for SEBS
1640	–OH bending
1465	Asymmetric deformation peak of $–CH_3$ and CH_2 and N–H deformation bending
1255, 1260	C–O stretching vibration
1044	Asymmetric Si–O–Si stretching
699	Styrenic C–H stretching

higher degree of grafting of both AA and MA (Figs. 1 and 2) in SEBS.

^{1}H NMR spectra of SEBS, AA-SEBS, and MA-SEBS are shown in Fig. 3a–c, respectively. From calculations, the ratio of styrenic to aliphatic peaks remains almost the same, 74:26 for neat SEBS (Fig. 3a). Since the concentration of the samples prepared for ^{1}H NMR in $CDCl_3$ has been kept exactly the same, the presence of peaks at 7.2 and 6.8 (characteristic for aromatic hydrogen) for AA-SEBS and MA-SEBS and having the same intensity as that of pristine SEBS (Fig. 3a) indicates that grafting has not taken place at the styrenic segment in any of the cases (Fig. 3b, c). The aliphatic secondary hydrogen is reacting in both the cases as indicated by the diminishing peak at $\delta = 1.57$. Peak area calculations around $\delta = 7.2$, 6.8 and 1.57 confirm that 6.2 and 3.8% grafting has been taken place in respective aliphatic moieties of AA6-SEBS and MA4-SEBS, respectively. This is in line with the values obtained from FTIR and chemical analysis.

Morphological investigation of AA and MA-grafted SEBS

Phase detected images in the tapping mode atomic force microscopy and bright field transmission electron microscopy exhibit well-ordered phase separated cylindrical-lamellar morphology consisting of bright nano-phasic domains corresponding to the hard PS component, and darker domains corresponding to softer rubbery ethylene-co-butylene (PEB) lamella for the triblock copolymer SEBS [16], as shown in Fig. 4a and b. This lamellar morphology gives a domain width of 19–23 nm for the bright areas of the styrenic nanophase and 12–15 nm for the softer ethylene-co-butylene phase of SEBS. This self-assembly of the block-copolymer SEBS is governed by a delicate balance between interaction energy and chain stretching. The repulsive interaction between the chemically different constituting blocks drives the system to phase separation, whereas the connectivity of the copolymer chains prevents macroscopic phase separation. As a result of this competing trend, SEBS self-organizes into complex structures like lamellar, cylindrical, hexagonal-packed cylinder, body-centered cubic sphere phases, etc. [16–18].

However, a morphological shift from a lamellar to spherical structure has been observed upon grafting with AA (3 and 6 wt %) of the poly-ethylene-butylene (PEB) micro domains. AFM and TEM images confirm this unique observation (Fig. 4c–d). Spherical PEB domains in AA-g-SEBS are evident from the TEM picture in Fig. 4c. The gross nature of the morphology remains as lamellar with occurrence of spherical PEB domains. The same patterns are obtained in both normal and parallel sections, confirming sphericity of PEB domains [18]. These nano-spherical domain sizes of AA-g-PEB range from 20 to 100 nm as appearing in 'tapping mode AFM' investigation in a relatively more clear morphology as revealed for AA-SEBS in Fig. 4d. The presence of hard and soft segments has been qualitatively investigated by force–distance (*f–d*) analysis by tapping mode AFM probe. The spherical patches give a larger hysteresis loop in-between tracking and re-tracking traces in *f–d* curve. This proves the softer behavior of these domains arising out of PEB mid-blocks. The harder domains show lesser adhesive nature (Fig. 4e–f). In our earlier publication, the quantitative analysis of jump-to-contact and pull-off forces by the AFM tip to the SEBS–clay nanocomposite surface has been discussed in detailed [30].

Figure 5a and b shows the AFM phase images of MA4-SEBS with occasional rubbery patches of dimensions of 30–60 nm with soft and hard tapping. Here, in this case, morphology is shifted from lamellar cylinders for pristine SEBS to short cylinders of PS and small patchy domains of PEB phases for MA-g-SEBS.

This morphological shift may be the result of an increase in the Flory–Huggins interaction parameter between the two blocks, a change in the volume fraction, and/or a loss of chain mobility resulting from hydrogen bonding after grafting. The viscoelastic study also revealed that two glass transition temperatures (T_gs) have been shifted on grafting (discussed later).

Mechanical and thermomechanical properties

High-strain mechanical properties of neat SEBS and grafted SEBS samples are reported in Table 4. On grafting SEBS by AA and MA, improved mechanical properties are achieved. AA3, AA6, MA2, and MA4-grafted SEBS matrices show improved tensile strength (6.3, 15.3, 11.5,

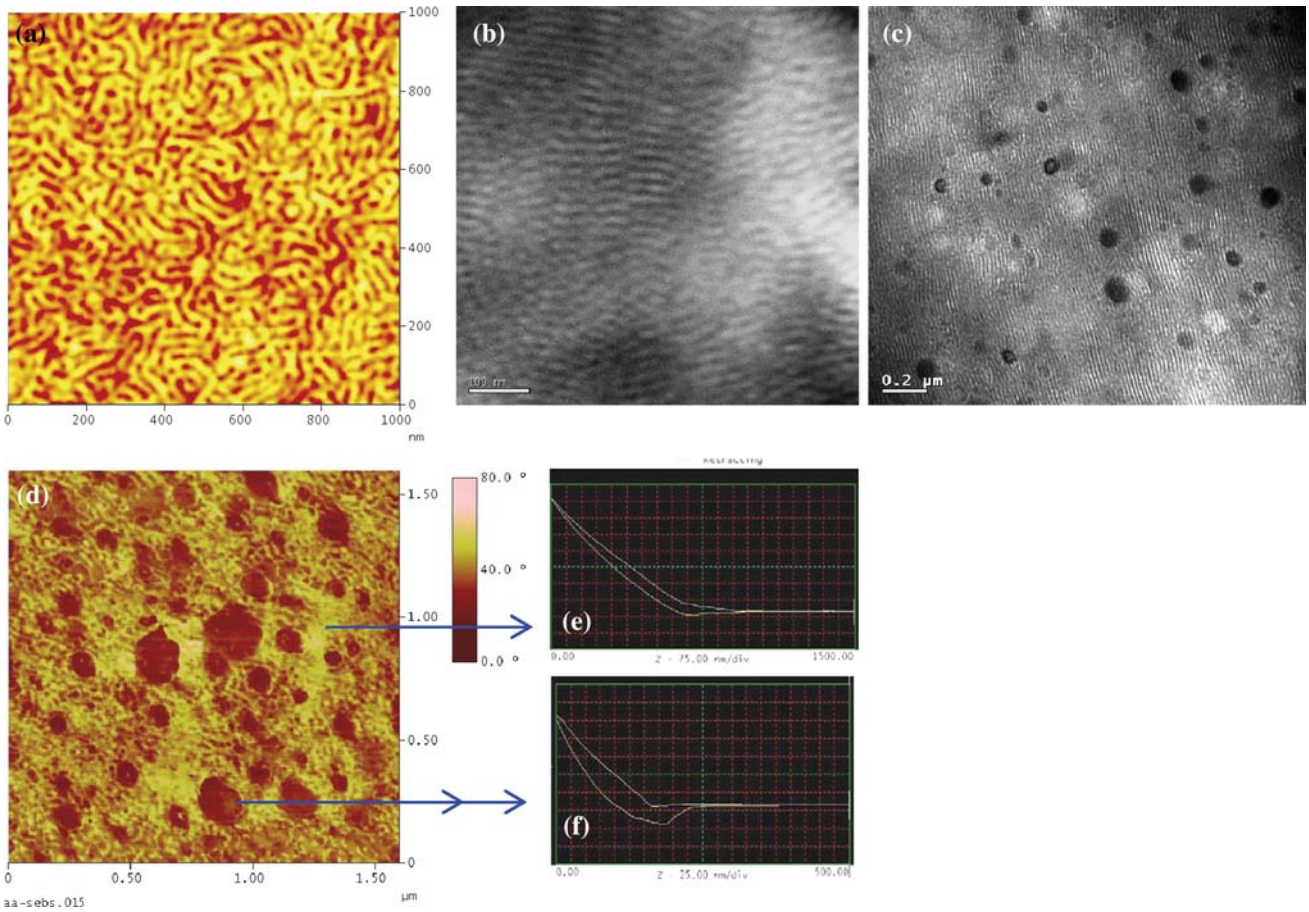

Fig. 4 Phase detected image of pristine SEBS in **a** tapping mode AFM and **b** bright-field TEM. Lamellar morphology with spherical domains for AA-g-SEBS from **c** TEM after selective staining by OsO_4, **d** AFM phase image of AA6-g-SEBS and force–distance plots taken on **e** hard and **f** soft segments in image (**d**)

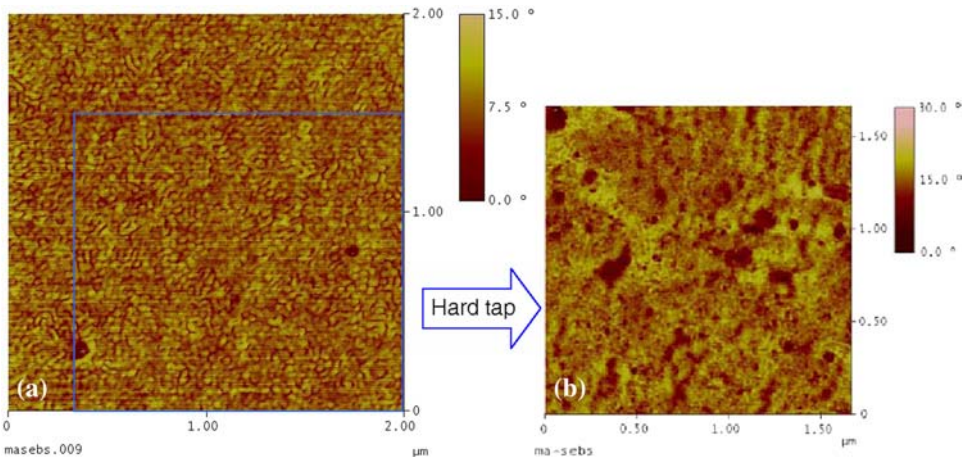

Fig. 5 Tapping mode AFM images of MA4-SEBS with alternating rubbery (*dark shade*) patches with **a** soft and **b** hard taping

and 14.8% respectively), modulus at 50% (3.8, 15.4, 3.8, and 15.4% respectively), and elongation at break (11.5, 11.5, 5.8, and 13.5% respectively), compared to the neat SEBS matrix. Among the grafted SEBS systems, MA4-SEBS and AA6-SEBS exhibit superior physico-mechanical properties compared to MA2 and AA3-SEBS and neat SEBS ones.

The dynamic measurement of the small-strain viscoelastic properties over a wide temperature range is a convenient approach to determine the phase organization in

Table 4 Tensile stress–strain of grafted SEBS-nanocomposites

Sample	Tensile strength (MPa)	Modulus at 50% strain (MPa)	Breaking elongation (%)
SEBS	23.6	2.6	520
AA3-SEBS	25.1	2.7	580
AA6-SEBS	27.2	3.0	580
MA2-SEBS	26.3	2.7	550
MA4-SEBS	27.1	3.0	580
SEBS-MT4	24.2	2.2	530
AA3-SEBS-MT4	26.8	2.9	570
AA6-SEBS-MT2	27.9	3.1	570
AA6-SEBS-MT4	33.5	3.6	620
AA6-SEBS-MT8	28.3	2.9	560
AA6-SEBS-OMT4	29.6	3.1	570
MA2-SEBS-MT4	28.1	2.7	580
MA4-SEBS-MT4	32.4	3.3	600
SEBS-OMT2	24.0	2.6	540
SEBS-OMT4	31.6	3.5	580
SEBS-OMT8	27.1	3.2	560

segmented copolymers. The AFM and TEM data have clearly shown that the copolymers present a phase separation (Fig. 4a–d). From the DMTA study, SEBS shows two glass transition temperatures (T_gs)—one at sub-ambient temperature (−52 °C) corresponding to a rubbery block and the other at post-ambient temperature (67 °C) corresponding to the plastic block (Fig. 6a, b). The viscoelastic study shows that in all cases of grafted SEBS, storage modulus increases, in line with the mechanical properties. Increase in rubbery tan δ peak height indicates that addition of pendant side groups in the mid-block of SEBS takes place in grafted SEBS. Figure 6a shows that AA6-SEBS has a higher rubbery tan δ position compared to SEBS, while this figure shows a lowering in the plastic tan δ peak. This is also the observation with MA2 and MA4 grafted SEBS (Fig. 6b).

Thermal degradation properties

On grafting of AA and MA moieties onto SEBS, considerable enhancement in thermal properties is observed as shown in Fig. 7a–c. On progressive grafting with 3 and 6 wt% of the AA moiety and 2 and 4 wt% of MAH, thermal stability increases as compared to pristine SEBS. The onset of degradation has progressively increased from 355 °C for pristine SEBS to 385 °C for AA3-SEBS. Maxima in the derivative curves (DTG) of the degradation profiles indicate the inflection points used to rank corresponding thermal stabilities. The degree of maleation onto SEBS has

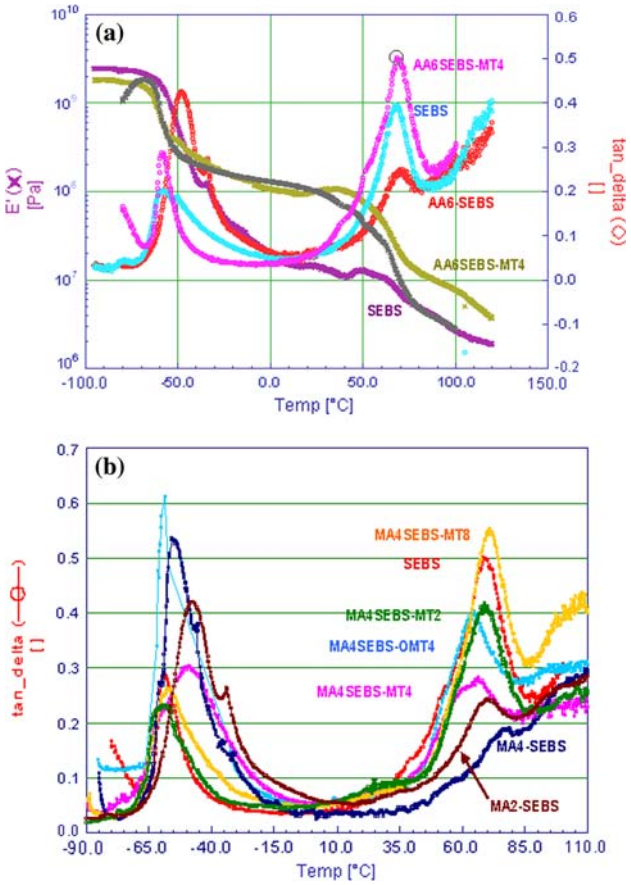

Fig. 6 Comparative storage modulus and tan δ trace for **a** SEBS, AA6-SEBS, and AA6-SEBS-MT4, **b** SEBS, MA2-SEBS, MA4-SEBS, and their MT and OMT-based nanocomposites

a prominent effect on enhanced thermal properties of maleated SEBS, which is revealed from Fig. 7b and c. More acrylation and maleation has imparted a higher thermal stability to the systems. Corresponding DTG maxima display that the height reduces as compared to neat SEBS for AA3-SEBS, AA6-SEBS, MA4-SEBS grafted polymers. This reduction in peak height indicates a reduction in the rate of degradation with the grafted species.

Effect of montmorillonite nanoclays on properties and morphology of grafted SEBS–clay nanocomposites

Microstructure by WAXD

In this investigation, hydrophilic moieties have been grafted in the form of AA and MA as characterized by FTIR and NMR measurements. Onto lightly grafted SEBS matrices, MT clay has been impregnated and their microstructure has been investigated by WAXD. The results are reported in Fig. 8 and Table 5. The peak corresponding to

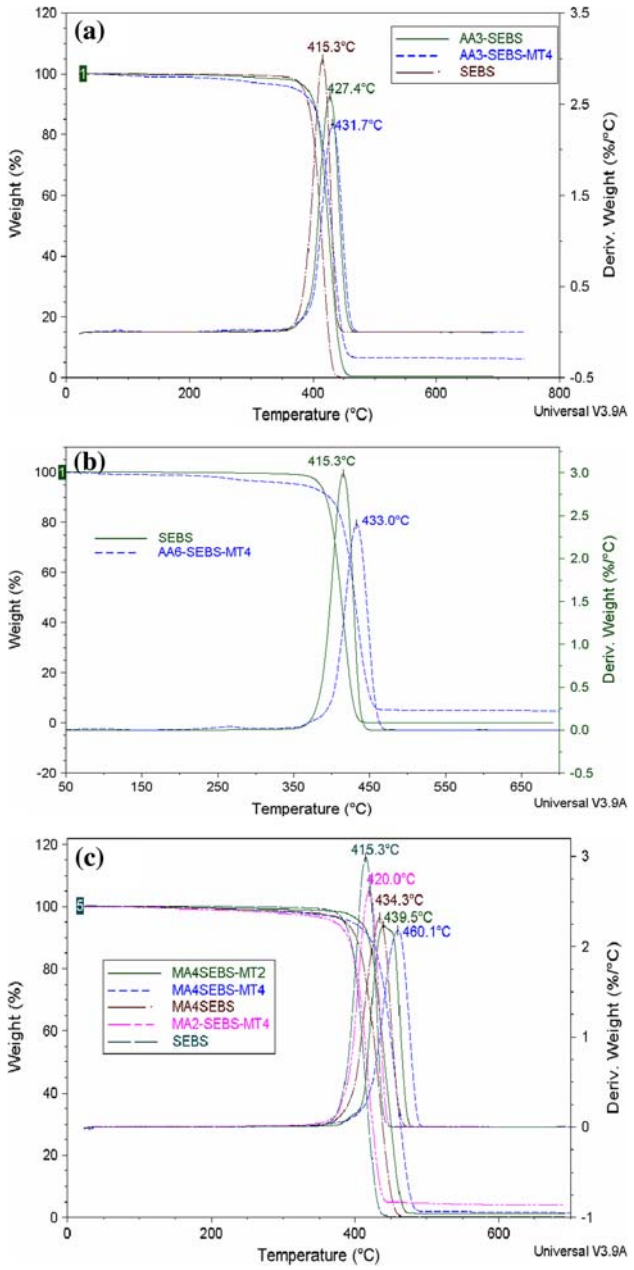

Fig. 7 Comparative TGA and DTG plots for **a** SEBS, AA3-SEBS, and AA3-SEBS-MT4, **b** SEBS, AA6-SEBS-MT4 and **c** SEBS, MA2-SEBS, MA4-SEBS, and their MT4-based nanocomposite

the 001 diffraction face of MT clays has been monitored for all the systems. The WAXD study shows that the *d*-spacing value for the SEBS-MT4, MA2-SEBS-MT4, and AA3-SEBS-MT4 systems is lower than that of the MA4-SEBS-MT4 and AA6-SEBS-MT4 nanocomposites (Table 5). Correspondingly, the peak height of the nanocomposites has gone down due to the presence of lower frequency (number) of stacked clay layers. The characteristic peak from MT plates in the WAXD has been fully diminished in the case of AA6-SEBS-MT2 and AA6-SEBS-MT4 nanocomposites (Fig. 8) and a very small hump corresponding to a very large gallery gap of almost 5 nm is observed for the MA4-SEBS-MT4 nanocomposite due to delamination of individual clay platelets in the entire matrix of grafted SEBS. These results are in line with the morphological studies presented in the next section. On increasing the loading of clay, however, agglomeration of clay layers occurs at 8 phr giving a stacked layer gap of 2.91 nm, as shown in Fig. 8.

The microstructure of the clay–polymer nanocomposite depends on the interactions between the nano-clay used and the polymer matrix. These interactions depend in turn on the 'polarity match' of the constituent. It has been shown by our previous study [29] that 4 wt% of unmodified MT clay gives a non-dispersed clustered (agglomerated) structure in the pristine SEBS matrix (Table 5 and TEM picture in Fig. 9a).

Microstructure of nanocomposites by AFM and TEM

On incorporation of MT clay in a pristine SEBS matrix, only agglomerated clusters are formed as shown in the TEM image in Fig. 9a. Proper dispersion of clay platelets could not be done in SEBS-MT mostly due to incompatibility of hydrophobic polymer with hydrophilic clay particles. After grafting, a good distribution of exfoliated MT clay platelets in an AA6-SEBS matrix and intercalated-exfoliated ones in MA4-SEBS matrix are observed in bright field TEM images (Fig. 9b, c). It is unique to have such a perfect exfoliation of individual clay layers with the unmodified MT clay at the same loading of 4 wt% in grafted SEBS matrices. Fine clays can be seen in the AFM three-dimensional phase image (Fig. 9c) of AA6-SEBS-MT4. This morphology is also seen by WAXD studies and is reflected in better physico-mechanical, optical, and thermal characteristics of these nanocomposites, as reported later.

Mechanical and thermomechanical properties

High-strain mechanical properties of neat SEBS, grafted SEBSs and their MT clay-based nanocomposites are reported in Table 4. Due to almost no intercalation of MT clays by SEBS, negligible improvement in physical properties results for SEBS-MT4 system. On grafting SEBS by AA and MA, much improved mechanical properties are achieved (Table 4), both for the polymer and for the MT-based nanocomposites. The best mechanical property is conferred by the AA6-SEBS-MT4 nanocomposite, which shows a tensile strength (TS) of 33.5 MPa and also an increase in elongation at break up to 620%. There is 23%

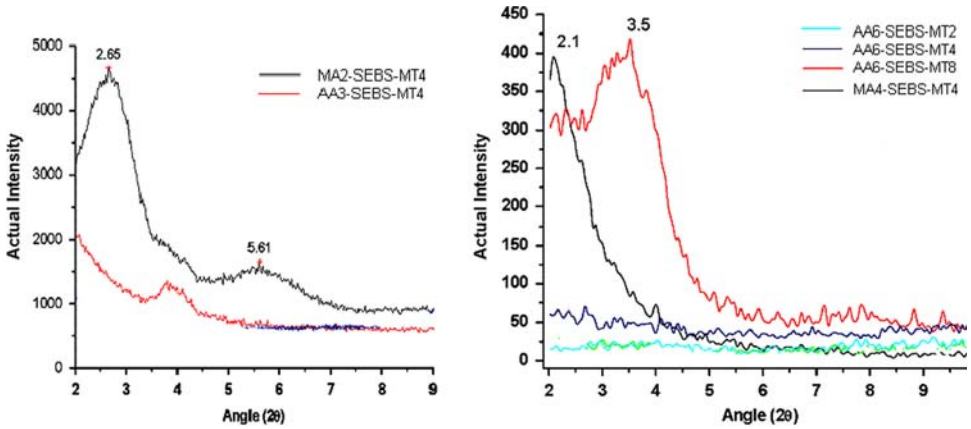

Fig. 8 X-ray diffraction pattern of MA and AA-grafted SEBS–MT nanocomposites

Table 5 XRD results of clay and clay-SEBS nanocomposites

Sample	2θ (°)	d-Spacing (nm)
MT clay	7.6	1.16
SEBS-MT4	6.4	1.38
AA3-SEBS-MT4	Very small hump at 3.6	Very few laminated spaces with 2.83
AA6-SEBS-MT2	–	Delaminated
AA6-SEBS-MT4	–	Delaminated
AA6-SEBS-MT8	3.5	Small agglomeration with 2.91
MA2-SEBS-MT4	2.65 and a small hump at 5.61	3.85 and small frequency with 1.82
MA4-SEBS-MT4	Small hump at 2.1	4.86
MA4-SEBS-OMT4	Peak at 3.5	2.91

improvement in tensile strength and 17% improvement in modulus for AA6-SEBS-MT4 system with respect to AA6-SEBS system, which has already shown improvement over neat SEBS. Forty percent improvements in TS and modulus are achieved for AA6-SEBS-MT4 with respect to values achieved for neat SEBS. On increasing the clay loading to 8 wt%, tensile strength and elongation at break drop in the case of AA6-SEBS-MT8, mostly due to re-lamination of clay stacks as evidenced from WAXD studies. On the other hand, better mechanical properties have been achieved on increasing the organically modified MT clays (OMT) in SEBS system. Optimum results are obtained with 4 wt% of OMT clay [29]. This OMT clay, however, does not impart best mechanical strength to the grafted AA6-SEBS. This can be explained by the higher affinity of the hydrophobic clay (OMT) toward the non-polar SEBS matrix, compared to lightly polar grafted SEBS (AA6-SEBS). MA4-SEBS provides higher strength than MA2-SEBS matrix, and so is the case with their corresponding nanocomposites based on MT4. MA4-SEBS-MT4 registers maximum strength among the maleated SEBS nanocomposites: tensile strength of 32.4 MPa, which means a 20% improvement with respect to MA4-SEBS. There is also a 600% increase in elongation at break. All these results are due to exfoliation-intercalation in the case of the modified systems and better dispersion of the clay platelets, as evidenced from the electron micrographs.

Viscoelastic properties of the grafted SEBS–clay nanocomposites are shown in Fig. 6a and b. The dynamic mechanical properties as a function of temperature are analyzed for the neat, grafted, and nanocomposite samples. After nanocomposite preparation, the position of the rubbery tan δ has moved toward positive temperatures, while the plastic tan δ peak height has increased with a gain in storage modulus in the plastic phase as seen for both AA6-SEBS-MT4 and MA4-SEBS-MT4 nanocomposites (Fig. 6a, b). Among 2, 4, and 8 wt% of MT clays, 4 wt% MT clay has shown to impart a maximum storage modulus for both MA4 and AA6 SEBS systems. At room temperature (25 °C), the E' value is highest for AA6-SEBS-MT4 followed by AA6-SEBS and neat SEBS (Fig. 6a). From the representative DMA traces, the compatibilization effect can be seen in the case of MA4-SEBS-MT4 and AA6-SEBS-MT4 nanocomposites.

Thermal degradation properties

Figure 7a–c portrays thermogravimetry (TG) and differential thermogravimetry (DTG) traces for pristine, grafted SEBSs, and their clay-based nanocomposites. Remarkable enhancement in thermal properties is observed on

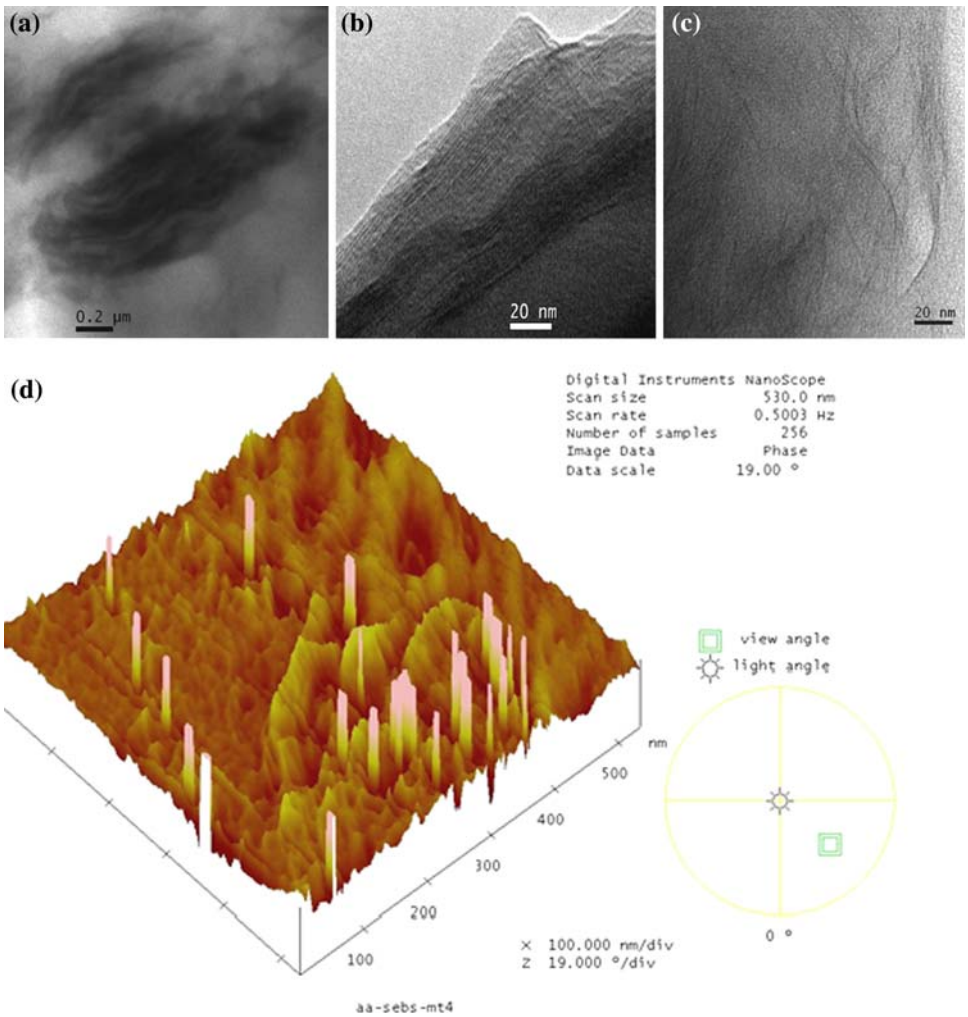

Fig. 9 Bright-field TEM morphology of **a** agglomerated SEBS-MT4, **b** intercalated-exfoliated mixed MA4-SEBS-MT4, and **c** exfoliated AA6-SEBS-MT4. Three-dimensional image by AFM showing **d** well-distributed clay in AA6-SEBS-MT4 nanocomposite

grafting onto SEBS, as discussed in the previous section. On synthesizing nanocomposites with these grafted SEBS based on MT clays, even further improvement in thermal stability is realized, as revealed from Fig. 7a–c. The onset of degradation has progressively increased from 355 °C for pristine SEBS to 385 °C for AA3-SEBS and further to 414 °C for AA3-SEBS-MT4. Figure 7b shows derivative curves (DTG) of degradation profiles. The maximum indicates the inflection point used to rank corresponding thermal stability. DTG maxima are seen to have improved much for the AA3-SEBS-MT4 nanocomposite (from 415 to 432 °C). In the case of the AA6-SEBS-MT4 nanocomposite, thermal stability is further enhanced as shown by the DTG maximum to 433 °C (Fig. 7c) and onset of degradation to 415 °C. Maximum rate of degradation is also reduced considerably in the case of the AA6-SEBS-MT4 nanocomposite as compared to SEBS.

Although AA6-SEBS shows a slight early weight loss probably due to the loss of smaller components from the grafted portions in SEBS, final thermal stability (i.e. T_{max}) is much improved both in AA3-SEBS and AA6-SEBS and their MT4-based nanocomposites. A total of 2 wt% of clay has less effect in enhancing thermal stability compared to 4 wt% clay. Though the DTG peak has shifted to 440 °C for MA4-SEBS-MT2, much improvement is achieved for MA4-SEBS-MT4 showing a DTG peak at 460 °C.

This improved thermal stability is possibly due to the rubbery phase getting modified by grafted moieties and subsequent incorporation of sodium montmorillonite nanoclay imparting a thermal barrier to degradation. The incorporation of unmodified clay into the grafted SEBS polymer matrix has tremendously enhanced the thermal stability by acting as a superior insulator and mass transport barrier to the volatile products generated during decomposition. Only 4 wt% of MT clay has imparted great thermal stability to these grafted SEBSs. As a consequence, the T_{max} (maxima in DTG plot) is also shifted to much higher temperatures and the height of this T_{max} has reduced considerably for AA3-SEBS-MT4, AA6-SEBS-MT4, and

MA4-SEBS-MT4 nanocomposites. The rate of degradation is also reduced at the maximum degradation zone as compared to their virgin component.

Optical transparency

Although layered silicates are microns in lateral size, they are just 1 nm thick. Thus, when single layers are dispersed (delaminated) in a polymer matrix, the resulting nanocomposite becomes optically clear in visible light. Figure 10a–c shows the appearance of the SEBS–MT nanocomposites with different filler contents. The samples have a thickness of 0.4 ± 0.1 mm and have been placed on the characters printed on paper. When MT clays are used in making the composite from neat SEBS, the light transmittance becomes so poor that this SEBS-MT4 becomes opaque in nature (Fig. 10a). This is simply because the MT clays cannot be dispersed in nano-dimension all throughout the SEBS matrix forming aggregates having dimensions more than the wavelength of the visible light wave front ($\lambda = 400$–700 nm). This indicates SEBS-MT4 cannot be termed as nanocomposite as incorporated clay layers do not stay in nano-dimensions ($\leq$100 nm). When lightly grafted SEBS is taken as matrix, superb retention of transparency (as in pristine SEBS) is achieved both with AA6-SEBS-MT4 and MA4-SEBS-MT4 nanocomposites (Fig. 10b, c). The characters under the composites become visibly clear, suggesting that the nanocomposites confer light transmittance in the visible wavelength region owing to small sizes of particulate dispersion throughout the matrix. Transmittance values from FTIR provide indication of retention of more than 85% transmittance even for filled nanocomposite samples.

Thermodynamics behind nanocomposite formation

The synergistically improved local and global effects (results of microscopy and mechanical–thermal properties respectively) obtained in this study can be explained in terms of thermodynamics behind the favorable mechanism of intercalation-exfoliation of clay galleries by SEBS. The free energy change of the system after mixing the clay in SEBS may be given as follows:

$$\Delta G_E = \Delta H_E - T\Delta S_E \quad \text{for elastomers} \tag{4}$$

$$\Delta G_C = \Delta H_C - T\Delta S_C \quad \text{for clays} \tag{5}$$

where E is the elastomer and C is the clay. Therefore, free energy change of the system on mixing of clay into the SEBS elastomer can be given as:

$$\Delta G_S = \Delta H_S - T\Delta S_S = \Delta H_S - T(\Delta S_E + \Delta S_C) \tag{6}$$

Every system seeks to achieve a minimum of free energy. In a reversible process, when Gibbs free energy becomes less than or equal to zero, the spontaneity of the reaction occurs in the said direction. From the expression in Eq. 4, the most favorable interaction between the clay and the rubber takes place when the ΔS_S value becomes positive, ΔH_S becomes negative or zero and hence ΔG_S also becomes negative, i.e. ≤ 0.

Intercalation of polymer chains in a clay gallery is exothermic in nature. In dispersed condition, a large number of solvent molecules need to be desorbed to accommodate polymer chains inside that gallery gap. The translational entropy gained by the system in this process provides the driving force for polymer adsorption on a clay surface. The entropy loss involved in confinement of SEBS polymer chains is not prohibitive to SEBS–clay hybrid formation. When polymer chains enter into the gallery of the clay, they reside in a restrained form. That is why ΔS_E tends to be negative. In contrast, the expansion of the gallery by elastomer chains causes entropy change in the clay, with ΔS_C to be positive [35]. Thus, an entropy gain associated with layer separation in exfoliated state counterbalances the entropy loss for confinement of polymer chain inside clay gallery gap, resulting in a net entropy change near to zero. Thus theoretically, the polymer–clay intercalation process depends on an energetic factor which in turn can be calculated from surface energies of the

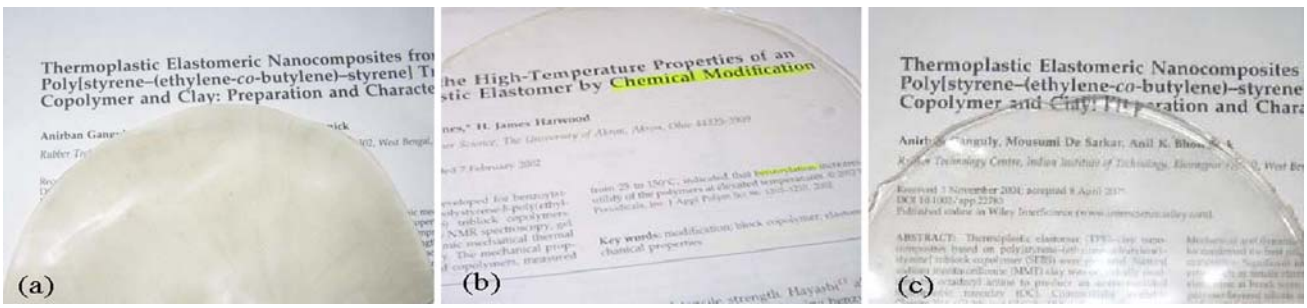

Fig. 10 Optical transmittance properties of composites: **a** opaque SEBS-MT4 agglomerated composite, **b** transparent AA6-SEBS-MT4, and **c** MA4-SEBS-MT4 nanocomposites

polymer and the clay. This energetic factor has been measured from a change of enthalpy (ΔH_S) on mixing clay with the polymer. ΔH_S can be calculated from the IR spectra of neat and nanocomposite samples using Fowkes' equation:

$$\Delta H_S = 0.236 * \Delta v \quad (7)$$

From Eq. 7, the driving force ΔH_S has been found to be negative for both MA4-SEBS-MT4 and AA6-SEBS-MT4 nanocomposites as shown in Table 6. A more negative ΔH_S value makes ΔG_S also more negative. A similar procedure has been followed by Maiti and Bhowmick [10]. In the case of SEBS-MT4, there is no IR peak shift from the FTIR of pristine MT, indicating lesser affinity among the constituents as compared to the aforesaid polar grafted SEBS–clay nanocomposite systems discussed. Hence, formation of MA4-SEBS-MT4 and AA6-SEBS-MT4 becomes more favorable than the SEBS-MT4 system.

Interfacial tension between the constituting polymer and MT clay of three representative nanocomposite systems has been measured from the static contact angle of two probe liquids. From Table 7, it transpires that the interfacial tension is lower for the AA6-SEBS and MA4-SEBS systems as compared to SEBS-based nanocomposites, explaining their easy formation compared to the latter one. In the proposed schematic model as shown in Scheme 3, hydrophilic modified SEBS chains at first adsorb on the extreme two free surfaces of MT clay layers. Then these two free surfaces get separated by shearing action. This process is repeated with the subsequent clay stacks. There is a simultaneous intercalation process reducing electrostatic interaction between the layers, thus facilitating exfoliation of clay galleries.

Table 6 Calculation of ΔH_S from IR peak shift

Sample	Peak position (cm^{-1})	ΔH_S (kcal mol^{-1})
MA4-SEBS	1712 and 1782	–
MA4-SEBS-MT4	1709 and 1779	−0.708
AA6-SEBS	1712	–
AA6-SEBS-MT4	1710	−0.478

Table 7 Interfacial tension of different SEBS–clay nanocomposites

Samples	Interfacial tension (mJ/m^2)
SEBS-MT4	1.46
MA4-SEBS-MT4	0.03
AA6-SEBS-MT4	0.63

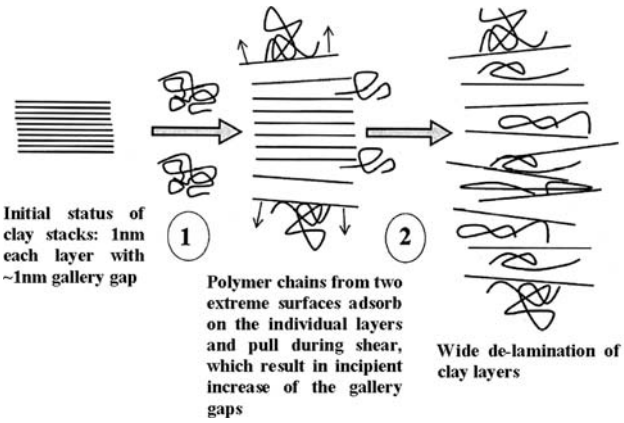

Scheme 3 Proposed schematic model of intercalation-exfoliation of clay platelets by polymer chains

Conclusions

1. SEBS was grafted by acrylic acid (3 and 6 wt%) and maleic anhydride (2 and 4 wt%) in solution and in a melt process, respectively. IR and NMR spectra confirmed that grafting had taken place at the mid-rubbery PEB blocks of SEBS in both the cases.
2. Grafted AA-SEBS and MA-SEBS showed superior physico-mechanical and thermal properties. On grafting, morphology was changed from purely cylindrical for neat SEBS to lamellar-spherical mixed one for the grafted SEBSs.
3. Unmodified montmorillonite clay (MT)-based nanocomposites were synthesized based on these grafted SEBS following solution intercalation process.
4. The dispersion of MT clays in neat SEBS matrix was a real problem as evidenced from morphology and reflected in its properties.
5. Hydrophilic MT clays were better dispersed and intercalated in these grafted SEBS matrices and MT clay-based nanocomposites gave better mechanical and thermal properties as compared to those of SEBS-MT and SEBS-OMT. AA6-SEBS-MT4 and MA4-SEBS-MT4 gave by far the best physico-mechanical properties. Forty percent improvements in TS and modulus were achieved for AA6-SEBS-MT4 over neat SEBS.
6. XRD and TEM studies revealed better interaction and dispersion of MT with the grafted-SEBS matrix resulting in better transparency of these nanocomposite films.
7. Remarkable improvements in thermal degradation were observed: 18 °C for AA6-SEBS-MT4 and 45 °C for MA4-SEBS-MT4.
8. Retention of optical transparency up to 85–90% as compared to pristine SEBS indicated very fine

dispersion of clay platelets in the entire matrices of AA-SEBS-MT4 and MA-SEBS-MT4 nanocomposites.

9. Thermodynamic calculations, interfacial tension, and a proposed schematic model explained a better exfoliation of unmodified MT clays in AA6-SEBS and MA4-SEBS.
10. From this study, it was proven that organic modification of clay is not mandatory in making polymer–clay nanocomposites. Polar modification of the SEBS matrix enabled cheaper MT clays to be used to synthesize excellent nanocomposites.

Acknowledgements AG acknowledges the scholarship grant in NDF category by AICTE, New Delhi, India. AKB is grateful to the Department of Science and Technology, New Delhi, for partially funding this project.

References

1. Pinnavaia TJ, Beall GW (eds) (2000) Polymer-clay nanocomposites. Wiley, New York
2. Giannelis EP, Krishnamoorti R, Manias E (1999) Adv Polym Sci 138:108
3. Giannelis EP (1996) Adv Mater 8:29
4. Vaia RA, Giannelis EP (1998) Macromolecules 30:8000
5. Morgan AB, Gilman JW (2003) J Appl Polym Sci 87:1329
6. Roy SS, Okamoto M (2003) Prog Polym Sci 28:1539
7. http://www.bccresearch.com/editors/rp-234r.html. Accessed 22 Jan 2007
8. Usuki A, Kojima Y, Kawasumi M, Okada A, Fukushima Y, Kurauchi T, Kamigaito O (1993) J Mater Res 8:1174
9. Kato M, Tsukigase A, Tanaka H, Usuki A, Inai I (2006) J Polym Sci A Polym Chem 44:1182
10. Maiti M, Bhowmick AK (2006) J Polym Sci B Polym Phys 44:162
11. Sadhu S, Bhowmick AK (2003) Rubber Chem Technol 76:0860
12. Sadhu S, Bhowmick AK (2004) J Polym Sci B Polym Phys 42:1573
13. Ren J, Silva AS, Krishnamoorti R (2000) Macromolecules 33:3739
14. Krishnamoorti R, Silva AS, Mitchell CA (2001) J Chem Phys 115:7175
15. Silva AS, Mitchell CA, Tse MF, Wang HC, Krishnamoorti R (2001) J Chem Phys 115:7166
16. Hamley I (ed) (1998) The physics of block copolymers. Oxford University Press, UK
17. Hasimoto H, Fujiyama M, Hasimoto T, Kawai H (1981) Macromolecules 14:844
18. Eirich FR (ed) (1978) Science and technology of rubber, 1st edn. Academic Press, New York
19. Heino M, Krjava J, Hietaoja R, Seppäla J (1997) J Appl Polym Sci 65:241
20. Weiss RA, Ashish S, Willis CL, Pottick LA (1991) Polymer 32:1867
21. Yarusso DJ, Cooper SL (1985) Polymer 26:371
22. Weiss RA, Lefelar JA (1986) Polymer 27:3
23. Storey R (1993) Polymer 34:4330
24. Mountz D (1998) Polym Chem Polym Preprs 39:383
25. Martins CR, Ruggeri G, De Paoli MA (2003) J Braz Chem Soc 14:797
26. Park B, Kong S, Kim Y, Jin N, Yong S (2005) Memburein 15:165
27. Mauritz K (2002) Polymer 43:4315, 5949
28. Lim ST, Lee CH, Kwon YK, Choi HJ (2004) J Macromol Sci B Phys 43:577
29. Ganguly A, DeSarkar M, Bhowmick AK (2006) J Appl Polym Sci 100:2040
30. Ganguly A, DeSarkar M, Bhowmick AK (2007) J Polym Sci B Polym Phys 45:52
31. Fowkes FM (1967) In: Patrick RL (ed) Treatise on adhesion and adhesives, vol 1. Marcel Dekker Inc., New York
32. Konar J, Sen AK, Bhowmik AK (1993) J Appl Polym Sci 48:1579
33. Ghosh P, Chattopadhyay B, Sen AK (1998) Polymer 39:193
34. Sen AK, Mukherjee B, Bhattcharya AS, De PP, Bhowmick AK (1992) Polym Degrad Stab 36:281
35. Chen B, Evans JRG (2005) Philos Mag 85:1519